International Journal of Nanoelectronics and Materials
Volume 16 (Special Issue) December 2023 [131-141]

Optimization of Gold Nanoparticles Electrodeposition Duration on Screen Printed Electrode to Enhance Electrochemiluminescence of Nitrogen-doped Carbon Dots

Nurul Izzati Akmal Mohd Azman[1], Nur Syakimah Ismail[1,2,*], Nur Hamidah Abdul Halim[3], Nurjuliana Juhari[1,2], Norhayati Sabani[1,2], Toibah Abd Rahim[4], Siti Aisyah Shamsudin[5] and Eiichi Tamiya[6]

[1]Faculty of Electronic Engineering & Technology, Universiti Malaysia Perlis (UniMAP), 02600 Arau, Perlis, Malaysia
[2]Centre of Excellence for Micro System Technology (MiCTEC), Universiti Malaysia Perlis (UniMAP), 02600 Arau, Perlis, Malaysia
[3]Institute of Nano Electronic Engineering (INEE), Universiti Malaysia Perlis (UniMAP), 02600 Arau, Perlis, Malaysia
[4]Faculty of Manufacturing Engineering, Universiti Teknikal Malaysia (UTeM), Melaka, Malaysia [5]Department of Applied Physics, Faculty of Science and Technology, Universiti Kebangsaan Malaysia, 43600, Bangi, Selangor, Malaysia
[6]Advanced Photonics and Biosensing Open Innovation Laboratory, AIST-Osaka University, Osaka University, 2-1 Yamadaoka, Suita, Osaka, 565-0871, Japan

ABSTRACT

In this work, the electrodeposition method was utilized to form gold nanoparticles on a carbon screen-printed electrode (SPE) using chronoamperometry at -0.4 V with various durations from 50 to 200 seconds. Scanning Electron Microscopy (SEM) images have proven that the electrodeposition method is capable of uniformly forming AuNPs on SPE (AuNPs-SPE). Apart from that, electrodeposition durations have increased the size of AuNPs by up to 66% based on average size measurements using ImageJ software. It can be observed that long electrodeposition durations permit the agglomeration of AuNPs on the electrode surface. The effect of electrodeposition duration on electrocatalytic performance in potassium ferricyanide and electrochemiluminescence (ECL) intensity of nitrogen-doped carbon dots (NCDs) was evaluated. Cyclic voltammetry (CV) of ferricyanide demonstrates that as the electrodeposition duration increases, AuNPs-SPE shows better electrochemical performance than bare SPE. ECL of NCDs displays that 100 s electrodeposition durations give the highest ECL intensity of 184% compared to bare SPE and have been chosen as the optimum parameter. The ECL mechanisms of bare SPE and AuNPs-SPE reveal that AuNPs-SPE has greater electrochemical and ECL performance than bare SPE, as evidenced by the CV of AuNPs-SPE having a faster reduction current, which rises to 87.2% ECL intensity and 510 mV faster ECL occurrence. These phenomena confirmed that the electrodeposition of AuNPs has improved the conductivity of SPE.

Keywords: Electrochemiluminescence, electrodeposition, gold nanoparticles, nitrogen-doped carbon dots, screen-printed electrode

1. INTRODUCTION

Carbon dots are an emerging member of the carbon allotrope. Nitrogen-doped carbon dots (NCDs) are a form of nanomaterial composed of carbon nanoparticles containing nitrogen ions. Element doping is more effective than surface passivation because it can alter the intrinsic properties of carbon dots, such as enhancing certain electrical and optical properties and increasing the number of active sites on the surfaces of carbon dots [1]. By doping carbon nanoparticles with electron-rich nitrogen atoms, it has been discovered that unique fluorescence

* Corresponding authors: syakimah@unimap.edu.my

phenomena and unexpected capabilities can be produced. NCDs exhibit strong fluorescence, emitting light in the visible spectrum. The wavelength of their emission can be shifted by revising the synthesis conditions or affecting the surface chemistry [2]. NCDs are beneficial for applications such as bioimaging, sensing, and optoelectronics due to their fluorescence properties. It is simple to modify the surface of nitrogen-doped carbon spots with various chemical groups. This allows them to be incorporated into complex systems or linked to biomolecules. This functionalization permits improved stability, biocompatibility, and specific interactions with molecules or cells of interest [3]. Consequently, fluorescent NCDs are anticipated to be excellent candidates for electrochemiluminescence (ECL) sensors [4–6].

Gold nanoparticles (AuNPs) play a significant role in the field of ECL, which combines electrochemistry and luminescence to enable sensitive and selective detection of analytes. AuNPs have been widely used to enhance the ECL signal due to their unique properties. To begin with, AuNPs can enhance ECL signals due to their excellent electrical conductivity and large surface-to-volume ratio. They can provide a large surface area for the immobilization of ECL species, thus amplifying the signal [7]. Moreover, AuNPs also serve as effective catalysts, enhancing the redox reactions involved in ECL [8]. Besides, AuNPs can act as sensitizers in the ECL system by accelerating the electron transfer process, generating more excited states, and leading to stronger light emission [9]. Furthermore, the incorporation of AuNPs into ECL systems can improve the stability of the system due to AuNPs resistance to photobleaching and other forms of degradation, which is crucial for maintaining a stable signal [10].

Electrochemical metal deposition offers a convenient and rapid approach to forming metal nanoparticles on large conductive surfaces through nucleation and growth processes. The reduction reaction of metal ions leads to the formation of tiny clusters of metal atoms called nuclei. The nuclei serve as sites for further gold ion deposition and growth [11]. There are two primary nucleation mechanisms namely instantaneous and progressive. Instantaneous nucleation involves the gradual growth of nuclei on a limited number of active sites that become activated simultaneously. On the other hand, progressive nucleation entails the rapid growth of nuclei on numerous active sites that become activated throughout the electroreduction process. [12]. Nevertheless, the catalytic performance of the metal nanoparticle-modified electrode depends on particle size and structure [13]. This attribute is governed by electrodeposition conditions such as method, durations, bulk concentrations, overpotential and many more [11,14].

Herein, we adopt the electrodeposition method to form AuNPs on screen-printed electrodes (AuNPs-SPE) through chronoamperometry method at various durations. We investigate the effect of electrodeposition durations on surface morphology, electrocatalytic activity and ECL of NCDs on AuNPs-SPE versus bare SPE. These outcomes will determine the optimum electrodeposition duration. Finally, we examined the ECL mechanism of NCDs on bare SPE and AuNPs.

2. MATERIAL AND METHODS

Citric acid ($C_6H_8O_7$), urea (CH_4N_2O), potassium persulfate ($K_2S_2O_8$) and potassium chloride (KCl), potassium ferricyanide ($K_3[Fe(CN)_6]$) were obtained from HmbG Trading Corporation, Malaysia. Tetrachloroauric(III) acid trihydrate ($HAuCl_4.3H_2O$) was purchased from Acros Organics, Belgium while hydrochloric acid (HCl) was acquired from Fisher Scientific (M) Sdn. Bhd. Phosphate buffer solution (PBS, 0.1 M, pH 7.4) was prepared using potassium phosphate dibasic (K_2HPO_4) and potassium phosphate monobasic (KH_2PO_4). All the chemicals were used as received.

The formation of NCDs and functional group were confirmed by Lambda 950 UV-Visible Spectrometer (PerkinElmer) and Spectrum 65 Fourier Transform Infrared (FT-IR) Spectrometer (PerkinElmer). The elements present in the sample were analyzed by Energy-Dispersive X-ray

(EDX) Spectroscopy (Tescan Vega). Scanning Electron Microscopy (SEM) was used to observe surface morphology of bare and AuNPs-modified SPE (AuNPs-SPE). Chronoamperometry (CA) and electrochemiluminescence (ECL) were performed using USB-powered Potentiostat (BDTeCL-XP; Biodevice Technology Co. Ltd., Japan) and data were collected using the uPMT-STAT V2 software as depicted in Figure 1. All electrochemical measurements used a screen-printed electrode (SPE) (EP-P; Biodevice Technology Co. Ltd., Japan). The three-electrode SPE system includes a carbon-based working electrode, a counter electrode, and an Ag/AgCI reference electrode. The working electrode surface of SPE is 2.64 mm2 [15]. A 30 µl electrolyte was applied directly onto the three-electrode surface and was discarded after a single use.

2.1 Synthesis of NCDs

10 mL of deionized (DI) water were used to dissolve a 3 g of citric acid and 3 g of urea. After that, this mixture was subjected to a 10-minute sonication process to completely dissolve the citric acid and urea into a colourless solution. The solution was then heated for 5 minutes at 800 watts in a domestic microwave to create a dark-brown, clustered solid known as nitrogen-doped carbon dots (NCD), which was subsequently baked for one hour at 60 °C in a pre-heated oven. The NCD samples was diluted with 20 ml of DI water and then sonicated for 10 minutes after the solution had cooled to room temperature. Finally, another 20 ml of DI water was added to the NCD solution before centrifuged at 3000 rpm for 20 minutes to remove agglomerated particles. The as-prepared NCD solution was stored at room temperature [16].

2.2 Electrodeposition of Gold Nanoparticles on SPE

1 mM HAuCl4 solution was prepared in 0.1 HCl (pH 1.2). The electrodeposition of AuNPs was performed through the chronoamperometry (CA) method at -0.4 V (vs Ag/AgCl) in 30 µL of the prepared solution, which covered all three electrodes on SPE [17]. Various electrodeposition durations were applied at 50, 100, 150 and 200 seconds. The gold nanoparticles-modified SPE (AuNPs-SPE) was rinsed using distilled water and blot-dried.

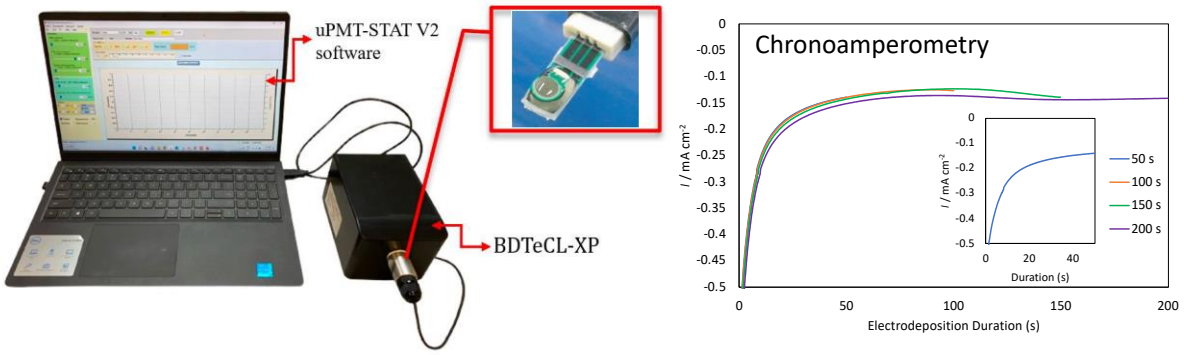

Figure 1. Electrodeposition of AuNPs on SPE setup.

2.3 Electrochemical and Electrochemiluminescence of NCDs Evaluation on Bare SPE and AuNPs-SPE

The electrochemical performance of bare SPE and AuNPs-SPE was evaluated using cyclic voltammetry (CV) in 2 mM $K_3[Fe(CN)_6]$ in 0.1 M PBS (pH 7.4) electrolyte. Optimization of electrodeposition durations to produce AuNPs-SPE was determined through the ECL intensity of NCDs that was conducted using CV of NCD in PBS with 0.1 M $K_2S_2O_8$ and 0.1 M KCl at a potential range of +2 to -2 V and a scan rate of 100 mV/s. Finally, ECL mechanisms of NCDs were investigated in PBS with 0.1 M KCl and PBS with 0.1 M $K_2S_2O_8$ and 0.1 M KCl through CV at a potential range of 0 to -2 V and a scan rate of 100 mV/s. For all ECL measurements, a 30x dilution of as-synthesized NCDs was used. Each parameter was repeated three times.

3. RESULTS AND DISCUSSION

3.1 Characterization of As-prepared Nitrogen-doped Carbon Dots

In Figure 2(a), it is evident that NCDs display an absorption peak at 273 nm, attributed to the characteristic aromatic π –π* transition, confirming the presence of a graphitic sp^2 carbon core [16]. Additionally, NCDs exhibit two clearly discernible absorption peaks at 338 nm and 408 nm. These peaks correspond to n–π* transitions, indicating the incorporation of oxygen and nitrogen groups that are bonded to the graphitic cores of the carbon dots [18-19]. As a consequence, NCDs was successfully synthesized through a microwave-assisted method, utilizing solely citric acid and the introduction of urea.

FTIR analysis was employed to offer insights into the molecular structure of NCDs. In Figure 2(b), a broad peak centered at 3284 cm^{-1} disclosing the presence of O-H and N-H bonds [18, 20]. Peaks at 1647 cm^{-1} and 1364 cm^{-1} correspond to C=O and CH_2 bonds, respectively, which are associated with the vibrational patterns of the benzene skeleton in conjugated sp2 carbon [18]. The absorption peak at 1204 cm^{-1} indicates the stretching vibration of C–N amines [4]. Consequently, it can be deduced that the surfaces of NCDs are enriched with hydroxyl and carbonyl groups, contributing to their water solubility. These findings also serve to validate the successful introduction of nitrogen into the carbon dots.

The elemental composition of NCDs was analyzed using EDX as feature in Figure 2(c). The weight percent (wt%) ratios of carbon (C), nitrogen (N) and oxygen (O) in the NCD were found to be 63.92, 18.88 and 17.20, respectively [19]. This EDX result proved that the as-synthesized material is a carbon-rich material that contains nitrogen and oxygen conjugated to the carbon graphitic cores, as revealed by UV-Vis and FTIR characterization.

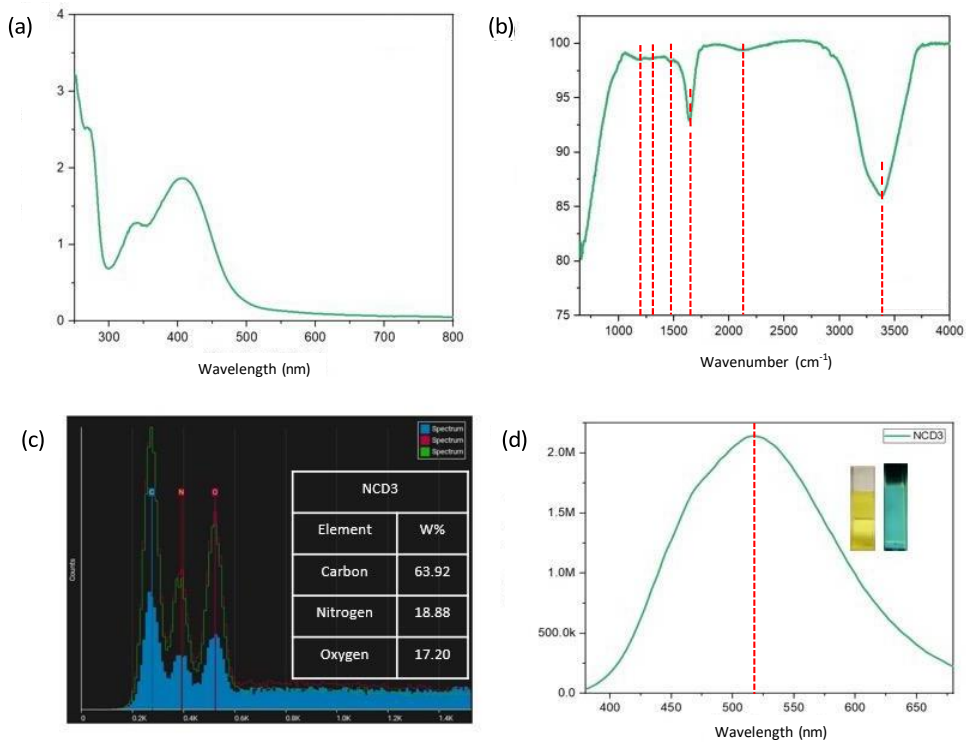

Figure 2. Characterization of NCDs through (a) UV-Vis, (b) FTIR, (c) EDX and (d) photoluminescence spectroscopy.

The emission wavelength and photoluminescent characteristics of carbon dots vary based on their size, which is a distinctive hallmark. Both from a foundational and practical perspective, the photoluminescence of carbon dots is an exceptionally captivating trait. Figure 2(d) shows the PL spectrum of NCD, while the insets are photographs of the aqueous solution of NCDs under ambient light and a UV lamp with a wavelength of 365 nm in dark conditions. The PL spectrum of NCDs revealed the maximum fluorescence emission peak was positioned at 517 nm after the excitation of a 365 nm laser source. The photograph of diluted NCDs shows a light brown color solution under normal light, which could also be easily observed with the naked eye, but emits a bright blue to almost green fluorescence color under a UV lamp [18]. This photograph's results match the obtained PL spectrum.

3.2 Surface Morphology of Electrodeposited Gold Nanoparticles on Screen-Printed Electrode

Figure 3(a) shows the SEM image of the working electrode area on SPE at 40X magnification where it is made of carbon paste. The bare surface of SPE is rough and flaky, as depicted by Figure 3(b). This bare SPE was then subjected to an electrodeposition process for the duration of 50, 100, 150 and 200 s in an acidic $HAuCl_4$ solution at -0.4 V. Then, the surface morphology observation and AuNP size measurement were conducted through SEM at 10000X magnification. Figure 3(c-f) shows circular bright spots on the working electrode of SPE, proving that AuNPs have successfully been deposited. Electrodeposition for the duration of 50 s has produced a non-uniform and random distribution of AuNPs, with a number of tiny particles coexisting with large nanocrystals. As the electrodeposition duration increased to 100 s, the electrode surface became dense with small monodispersed AuNPs that evenly distributed. An electrodeposition duration of 150 s yields a compact distribution with large AuNPs, whereas 200 s produces loosely distributed AuNPs with bigger cluster sizes.

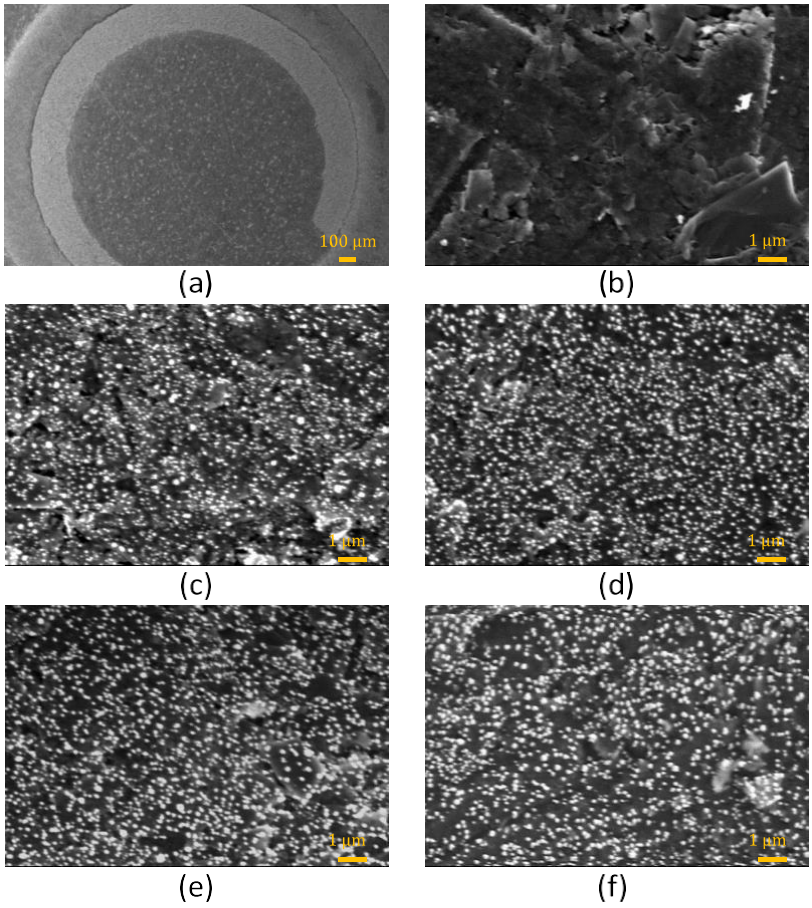

Figure 3. SEM images of (a) working electrode of carbon screen-printed electrode with (b) 0 s, (c) 50 s, (d) 100 s, (e) 150 s and (f) 200 s electrodeposition duration.

Subsequently, ImageJ software was used to analyze SEM images of AuNPs-SPE to obtain the average size of AuNPs at 10 random selection points. Figure 4 shows that the electrodeposition durations of 50 s produce an average size of 89.57 nm and increase by 13.5%, 40% and 66% as electrodeposition durations rise to 100, 150 and 200 s, respectively. Based on SEM images and average size evaluation, long electrodeposition durations increase AuNP size while decreasing particle density. The increase in size is attributed to the growth of initially formed nuclei and progressive nucleation, while the decrease in particle density is due to the growth and coalescence of neighboring Au particles that subsequently promote the agglomeration of AuNPs [21].

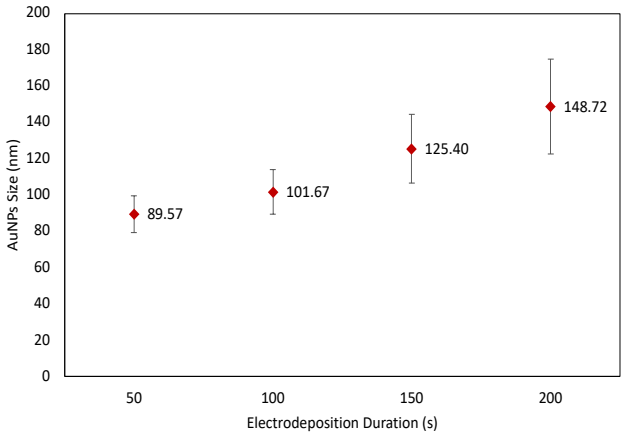

Figure 4. Size of AuNPs subjected to various electrodeposition durations.

3.3 Optimization of Gold Nanoparticles Electrodeposition Duration

To begin with, the electrocatalytic characteristics of bare SPE and AuNPs-SPE produced from various electrodeposition durations as electrochemical sensors were investigated by CV from -0.8 to 0.8 V at a scan rate of 100 mV/s in the solution containing 2 mM $K_3[Fe(CN)_6]$ in PBS, as depicted by Figure 5. Then, oxidation peak current (I_p), oxidation peak potential (E_{ox}), reduction peak potential (E_{red}) and peak-to-peak separation of redox signal ($DE_{p\text{-}p}$, obtained from E_{ox}-E_{red}) values were extracted from the CV and listed in Table 1. An increase in electrodeposition duration has linearly increased the I_p values, which represent the conductivity of AuNPs-SPE in comparison to bare SPE. CVs display the onset oxidation potential of ferrocyanide to ferricyanide at -0.05 V and the onset reduction potential of ferricyanide to ferrocyanide at 0.24 V for all electrodes. However, each electrode has different oxidation and reduction rate performance based on electrodeposition duration. Based on E_{ox} and E_{red}, AuNPs- SPE with an electrodeposition duration of 200 s demonstrated the fastest oxidation rate, while bare SPE showed the fastest reduction rate. This result also indicates that AuNPs-SPE might hinder the reduction of ferricyanide to ferrocyanide as smaller E_{red} values are observed compared to bare SPE. Apart from that, $\Delta E_{p\text{-}p}$ of bare SPE shows lower reversible electron transfer compared to AuNPs-SPE formed at 50 to 150 s electrodeposition duration. Yet, AuNPs-SPE with a 200 s electrodeposition duration demonstrates the lowest $\Delta E_{p\text{-}p}$ values that represent the fastest electron transfer kinetics between electrode and analyte. This outcome might be due to the morphology of AuNPs that are enriched with active crystallographic faces, which exhibit better kinetic and electrocatalytic activity [21]. Overall, the electrocatalytic performance of AuNPs-SPE at all electrodeposition durations shows significant improvement compared to bare SPE, especially in terms of I_p and E_{ox}.

After confirming that AuNPs-SPE has better electrochemical performance than bare SPE, the ECL of NCDs was measured through a co-reactant pathway with potassium persulfate ($K_2S_2O_8$) at a potential range of +2 to -2 V. Figure 6 shows that bare SPE emits an ECL intensity of 1760. AuNPs-SPE with electrodeposition durations of 50 s and 100 s has increased ECL intensity emission by 2.1% and 184%, respectively. AuNPs-SPE produced from longer electrodeposition durations of 150 and 200 s has reduced ECL intensity emission by 27.2% and 43.2%, respectively, in comparison to AuNPs-SPE made from a 100 s electrodeposition duration. This result shows that AuNPs-SPE with a 100 s electrodeposition duration has the most effective electroreduction of NCDs and $K_2S_2O_8$ to generate CDs and peroxydisulfate radicals that simultaneously increase ECL intensity. Therefore, AuNPs-SPE produced from a 100 s electrodeposition duration has been chosen as the optimum parameter.

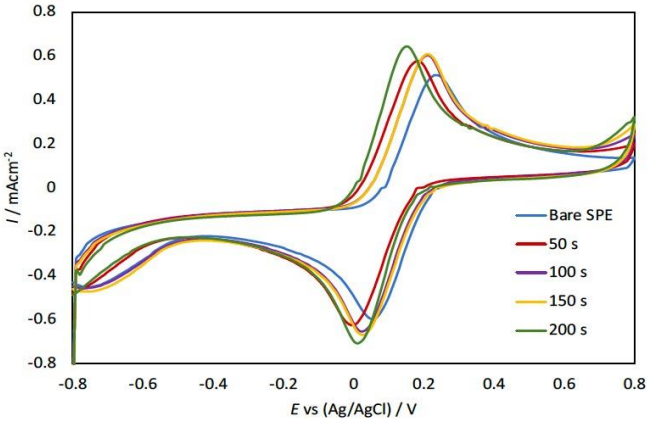

Figure 5. CV of bare SPE and AuNPs-SPE with various electrodeposition durations in 2 mM $K_3[Fe(CN)_6]$ in 0.1 M PBS.

Table 1 Electrocatalytic evaluation of AuNPs-SPE

Electrodeposition Duration	I_p (mAcm^{-2})	E_{ox} (V)	E_{red} (V)	ΔE_{p-p} (V)
Bare SPE	0.512	0.230	0.060	0.163
50 s	0.572	0.180	0.000	0.180
100 s	0.604	0.210	0.030	0.180
150 s	0.606	0.210	0.030	0.185
200 s	0.635	0.150	0.010	0.140

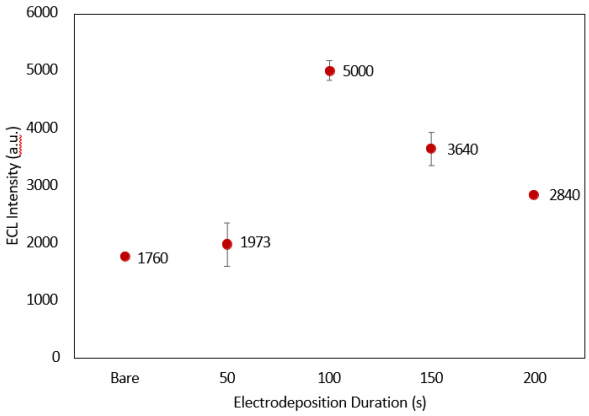

Figure 6. ECL intensity of bare SPE and AuNPs-SPE with various electrodeposition durations in NCDs + 0.1 M $K_2S_2O_8$ + 0.1 M PBS + 0.1 M KCl.

3.4 Electrochemiluminescence Mechanism of NCDs on Bare SPE versus AuNPs-SPE

Figure 7 displays the CVs and ECL intensities of NCDs on bare SPE and AuNPs-SPE made of 100 s electrodeposition duration in electrolyte with and without co-reactant $K_2S_2O_8$ (inset). The CV of bare SPE NCDs + 0.1 M KCl + 0.1 M PBS shows two distinct peaks at -0.63 V and -1.35 V during reverse scan that belong to the reduction of NCDs to form $CD^{\bullet-}$ (equation 1) and oxygen evolution,

respectively (inset of Figure 7(a)). Meanwhile, AuNPs-SPE only shows one distinct peak at -0.57 V and a rapid reduction current before continuing with an forward scan. This result demonstrates that AuNPs-SPE has a 60 mV faster reduction peak potential for NCDs compared to bare SPE. However, this CV resulted in no emission of luminescence from the NCD, as observed in the inset of Figure 7(b). This phenomenon proved that the annihilation pathway reaction did not happen to create ECL emissions of NCDs either at reverse or forward scan.

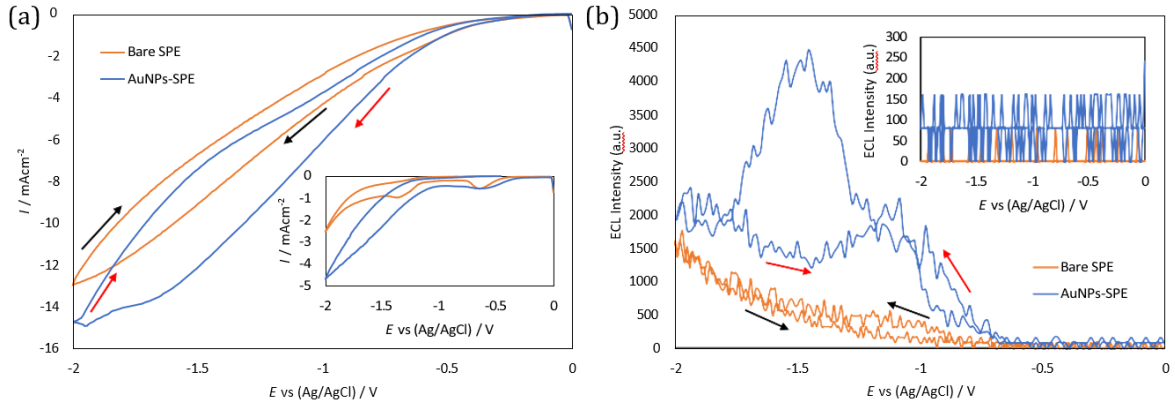

Figure 7. (a) CV and (b) ECL of bare SPE and AuNPs-SPE with 100 s electrodeposition duration in NCDs + 0.1 M $K_2S_2O_8$ + 0.1 M PBS + 0.1 M KCl. Insets are CV and ECL of bare SPE and AuNPs-SPE in NCDs + 0.1 M PBS + 0.1 M KCl.

Afterwards, the ECL reactions of bare SPE and AuNPs-SPE in NCDs + 0.1 M $K_2S_2O_8$ + 0.1 M PBS + 0.1 M KCl electrolyte were inspected for co-reactant pathway reactions between NCDs and $K_2S_2O_8$. CV of bare SPE and AuNPs-SPE displays rapid current reduction with onset reduction potential at -0.55 V during reverse scan, but no distinct peaks for NCDs or $K_2S_2O_8$ reduction were observed, which might suggest that both species reduce simultaneously to form $CD^{\bullet-}$ and $SO_4^{\bullet-}$ radicals (Figure 7(a)) as per equation 1 and 2. The resultant ECL intensities show that both bare SPE and AuNPs-SPE are capable of emitting luminescence through the co-reactant pathway from $CD^{\bullet-}$ and $SO_4^{\bullet-}$ reaction to excited states of CD^*, as per equation 3 and 4 [4,16]. The highest ECL intensity of AuNPs-SPE occurs at -1.44 V, whereas the ECL of bare SPE appears at -1.95 V during reverse scan that rapidly produces the excited states of CD^* (Figure 7(b)). During forward scan, the ECL intensity slowly depleted until all $CD^{\bullet-}$ and $SO_4^{\bullet-}$ radicals were completely consumed. It can be clearly observed that the CV of AuNPs-SPE has a more rapid reduction current that consequently increases in 87.2% ECL intensity and 510 mV faster ECL occurrence, proving that AuNPs act as catalysts to form fast and abundant $CD^{\bullet-}$ and $SO_4^{\bullet-}$ radicals that result in better electrochemical and ECL performance of AuNPs-SPE in comparison to bare SPE.

$$CD + e^- \rightarrow CD^{\cdot-} \quad (1)$$

$$S_2O_8^{2-} + e^- \rightarrow SO_4^{\cdot-} + SO_4^{2-} \quad (2)$$

$$SO_4^{\cdot-} + CD^{\cdot-} \rightarrow CD^* + SO_4^{2-} \quad (3)$$

$$CD^* \rightarrow CD + \hbar\nu \quad (4)$$

4. CONCLUSION

NCDs have been synthesized through a microwave-assisted method using citric acid and urea. UV-Vis, FTIR and EDX have confirmed that the nitrogen element has been doped to the graphitic carbon and contains hydroxyl and carboxylic groups that make the NCDs hydrophilic. The electrodeposition method has been adopted to produce AuNPs on the working electrode of SPE at various durations ranging from 50 to 200 s. SEM images display a uniform formation of AuNPs on the electrode surface with increased density and size as the electrodeposition duration increases. The electrocatalytic activity of bare SPE and AuNPs-SPE has been investigated in ferricyanide solution, which shows that with increasing electrodeposition duration, AuNPs-SPE has better electrochemical performance. The ECL of NCDs on AuNPs-SPE that were subjected to 100 s electrodeposition durations has shown superior ECL intensity compared to other electrodes and has been chosen as the optimum parameter. Further inspection of the ECL mechanism of NCD on bare SPE and AuNPs-SPE reveals that only co-reactant pathways can produce luminescence emission from $CD^{\bullet-}$ and $SO_4^{\bullet-}$ radicals. AuNPs-SPE, which produces 87.2% ECL intensity and 510 mV more positive ECL potential, has proven to have better electrocatalytic activity than bare SPE.

ACKNOWLEDGEMENTS

The author would like to acknowledge the support from the Fundamental Research Grant Scheme for Research Acculturation of Early Career Researchers (FRGS-RACER) under a grant number of RACER/1/2019/STG07/UNIMAP//1. A huge appreciation to Prof. Eiichi Tamiya from Osaka University for lending us ECL measurement instrument to carry out this research. We gratefully acknowledge the assistance of Mr. Mohammad Isa Ahmad Azan from the Institute of Nano Electronic Engineering, UniMAP in the SEM characterization of AuNPs-SPE.

REFERENCES

[1] Liang, S., Wang, M., Gao, W., Zhao, X., Optical Materials vol. 128 (2022) pp.112471.
[2] Wang, X., Zhang, M., Huo, X., Zhao, W., Kang, B., Xu, J. J., Chen, H., Nanoscale Adv. vol 1, issue 5 (2019) pp.1965-1969.
[3] Nair, A., Haponiuk, J. T., Thomas, S., Gopi, S., Biomedicine & Pharmacotherapy vol. 132 (2020) pp.110834.
[4] Fiorani, A., Merino, J. P., Zanut, A., Criado, A., Valenti, G., Prato, M., Paolucci, F., Current Opinion in Electrochemistry vol. 16 (2019) pp.66-74.
[5] Jampasa, S., Ngamrojanavanich, N., Rengpipat, S., Chailapakul, O., Kalcher, K., Chaiyo, S., Biosensors and Bioelectronics vol. 188 (2021) pp.113323.
[6] Li, Y., Li, R., Zhu, Z., Liu, J., Pan, P., Qi, Y., Yang, Z., Microchemical Journal vol. 183 (2022) pp.108073.
[7] Shi, X., Liu, H., Zhang, M., Yang, F., Li, J., Guo, Y., Sun, X., Sensors and Actuators B: Chemical vol. 348 (2021) pp.130663.
[8] Bezuneh, T. T., Fereja, T. H., Kitte, S. A., Li, H., Jin, Y., Talanta vol. 248 (2022) pp.123611.
[9] Liu, P., Wang, L., Zhao, K., Liu, Z., Cao, H., Ye, S., Liang, G., Sensors and Actuators B: Chemical vol. 316 (2020) pp.128131.
[10] Liu, Y., Zhang, H., Li, B., Liu, J., Jiang, D., Liu, B., Sojic, N., J. Am. Chem. Soc. vol. 143, issue 43 (2021) pp.17910-17914.
[11] Hezard, T., Fajerwerg, K., Evrard, D., Collière, V., Behra, P., Gros, P., Electrochimica Acta vol. 73 (2012) pp.15-22.
[12] Grujicic, D., Pesic, B., Electrochimica Acta vol. 47 (2002) pp.2901-2912.
[13] Tang, Y., Cheng, W., Langmuir vol. 29, issue 9 (2013) pp.3125-3132.

[14] Finot, M. O., Braybrook, G. D., McDermott, M. T., J. Electroanal. Chem. vol. 466 (1999) pp.234- 241.
[15] Ismail, N. S., Hoa, L. Q., Huong, V. T., Inoue, Y., Yoshikawa, H., Saito, M., Tamiya, E., Electroanalysis vol. 29, issue 4 (2017) pp.938-943.
[16] Azman, N. I. A. M., Halim, M. A. A. A., Ismail, N. S., Halim, N. H. A., Juhari, N., Sabani, N., Shamsudin, S. A., Tamiya, E., Int. J. Nanoelectronics and Materials vol. 16, issue 4 (2023) article in press.
[17] Chikae, M., Idegami, K., Kerman, K., Nagatani, N., Ishikawa, M., Takamura, Y., Tamiya, E., Electrochemistry Communications vol. 8 (2006) pp.1375-1380.
[18] Qu, S., Wang, X., Lu, Q., Liu, X., Wang, L., Angew. Chem. Int. Ed. vol 51, issue 49 (2012) pp. 12215-12218.
[19] Holá, K., Sudolská, M., Kalytchuk, S., Nachtigallová, D., Rogach, A. L., Otyepka, M., Zbořil, R., ACS Nano vol. 11, issue 12 (2017) pp.12402-12410.
[20] Arcudi, F., Dordevic, L., Prato, M., Angew. Chem. Int. Ed. vol 55, issue 6 (2016) pp.2147-2152.
[21] El-Deab, M.S., Electrochimica Acta vol. 54 (2009) pp.3720-3725.